A novel heat recovery for a marine diesel engine with power and cooling outputs; exergetic, economic, and net present value investigation and multi-criteria NSGA-II optimization

Yan Cao [a], Mohamed Salem [b,*], Samia Nasr [c], Shayma Hamza Sadon [d], Pradeep Kumar Singh [e,*], Azher M. Abed [f,*], Mahidzal Dahari [g,*], Maha M. Almoneef [h], Makatar Wae-hayee [i,*], Ahmed M. Galal [j,k]

[a] School of Computer Science and Engineering, Xi'an Technological University, Xi'an, 710021, China
[b] School of Electrical and Electronic Engineering, Universiti Sains Malaysia (USM), Nibong Tebal, 14300 Penang, Malaysia
[c] Advanced Functional Materials Laboratory (AFMQL),Department of Physics, Faculty of Science, King Khaled University, P.O. Box 9004, Abha, Saudi Arabia
[d] Department of Petroleum &Mining Engineering, The Faculty of Engineering, Tishk International University, Erbil, Kurdistan Region-Iraq
[e] Department of Mechanical Engineering, Institute of Engineering & Technology, GLA University, Mathura, U.P. 281406, India
[f] Air conditioning and Refrigeration Techniques Engineering Department, Al-Mustaqbal University College, Babylon 51001, Iraq
[g] Deparment of Electrical Engineering, Faculty of Engineering, Universiti Malaya, 50603, Kuala Lumpur, Malaysia
[h] Physics Department, Faculty of Science, Princess Nourah bint Abdulrahman University, Riyadh, Saudi Arabia
[i] Department of Mechanical and Mechatronics Engineering, Faculty of Engineering, Prince of Songkla University, Hatyai, Songkhla, 90110, Thailand
[j] Department of Mechanical Engineering, College of Engineering in Wadi Alddawasir, Prince Sattam bin Abdulaziz University, Saudi Arabia
[k] Production Engineering and Mechanical Design Department, Faculty of Engineering, Mansoura University, P.O 35516, Mansoura, Egypt

ARTICLE INFO

ABSTRACT

Owing to the marine environmental pollution affected by cruises, the use of techniques to mitigate carbon dioxide emission (CO_2) is vital. Since a quarter of the fuel energy input to the engine is lost, waste management for marine diesel engines can provide some valuable outputs by which the need for other energy conversion-based methods disappears. Hence, the current work proposes a novel model of waste heat recovery for a 1 MW marine diesel engine in a low-temperature framework by which outstanding results are predictable. The defined auxiliary model consists of an absorption power cycle and an ejector refrigeration cycle to produce useful electricity and cooling for air conditioning. This model is designed for the first time and comprehensively analyzed and optimized to set the most suitable state of operation. The potential of the model is measured through the exergy, environmental, economic, and net present value standpoints. Moreover, an advanced evolutionary algorithm based on the non-dominated sorting genetic algorithm-II is applied to reach the optimum cost and exergetic performance. The optimum state showed an exergy efficiency of 35.19 % and products' specific cost of 53.01 \$/GJ. Moreover, the optimum payback period and CO_2 emission reduction equal 6.79 years and 21.5 kg/MWh, respectively.

1. Introduction

The energy demand has unprecedentedly faced an increase with changing the structure of social life and policy-making of countries in recent decades [1–8]. This statement can be generalized to all aspects of human needs, e.g., industry, agriculture, urban interactions, travel, etc. [9–15]. Consequently, fuel consumption, especially fossil and hydrocarbon fuels, has augmented exponentially, increasing fuel costs and severe environmental issues [16–20]. According to previous studies, industrial applications lead to almost 60 % waste of energy during heat transfer- and combustion-based processes [21]. It is estimated that around 80 % of total energy loss takes place in low temperatures, where

* Corresponding authors.
E-mail addresses: salemm@usm.my (M. Salem), pradeep.kumar@gla.ac.in (P. Kumar Singh), mahidzal@um.edu.my (M. Dahari), wmakatar@eng.psu.ac.th (M. Wae-hayee).

Nomenclature

AI	Annual income,
AS	Annual saving,
c	Specific cost , /GJ
CI	Cost index
$\dot{C}$	Cost rate, /h
CRF	Capital recovery factor, −
CER	CO_2 emission reduction , kg/MWh
DC	Direct cost,
$\bar{ex}_m^{ch,o}$	Chemical molar standard exergy, kJ/kmol
FC	Fixed cost,
h	Specific enthalpy, kJ/kg
i_r	Interest rate, −
IC	Indirect cost,
IF	Inflation factor, %
$\dot{I}_D$	Exergy destruction rate, kW
$\dot{I}_F$	Fuel exergy rate, kW
$\dot{I}_L$	Exergy loss rate, kW
$\dot{I}_P$	Product exergy rate, kW
M	Molar mass, kg/kmol
$\dot{m}$	Mass rate, kg/s
$\dot{n}$	Molar rate, kmol/s
n	Components lifetime, year
N	Yearly time of operation , h
NPV	Net present value,
OC	Cost of operation ,
P	Pressure, bar
$\dot{Q}$	Thermal energy rate, kW
R	Universal gas constant, kJ/kmol K

RDM	Real discount factor, %
S_i^+	Distance between each point and the best point
S_i^-	Distance between each point and the worst point
T	Temprture, K
ΔT	Temperature difference, K
U	Overall heat loss coefficient, $kW/m^2 K$
v_j^+	Ideal value of the jth objective
v_j^-	Non − deal value of the jth objective
$\dot{W}$	Power, kW
y	Molar fraction, −
$\dot{Z}_k$	Investment cost rate, /h
Z_k	Purchase cost, /h

Greek Symbols

ψ	Exergy rate, kW
η_{en}	Energetic efficiency , %
η_{ex}	Exergetic efficiency , %
η_{is}	Isentropic efficiency, %
φ	Maintenance factor, −

Subscripts

0	Reference state
F	Fuel
in	Inlet
k	kth component
net	Net value
out	Outlet

diesel engines have the highest contribution to waste, almost 58 % [22]. Subsequently, the waste heat recovery (WHR) technology has been proposed by which the relevant issues of performance, cost, and environment have partially been adjusted [23–28]. The improvement of the performance of diesel engines having a variety of use in different industries is vital for better applications. Some studies have addressed this issue and surveyed the WHR of diesel engines [29].

Sadeghi et al. [30] comparatively investigated the applicability of an absorption chiller and an ERC to recover the waste heat of a diesel engine. It was predicated that the ERC is a better coolant from the cost standpoint with a unit cost of 201 $/GJ. Also, it enhanced the exergetic efficiency of the scheme by 15.2 % at the optimum state. Xia et al. [31] used a configuration of a supercritical Brayton cycle (SBC), an organic Rankine cycle (ORC), and an ejector refrigeration cycle (ERC) recovering the heat wasted by a diesel engine. Their optimization endeavor led to an exergetic efficiency of 27.6 % and products' specific cost of 63.5 $/MWh. In a study by Yang et al. [32], they recovered the waste heat of a diesel engine with an ORC through an experimental setup. The experimental results were evaluated using an artificial neural network (ANN) and optimized via a genetic algorithm by an error below 5 %. The WHR for a diesel engine was done and optimized by Habibi et al. [33] utilizing a combined cycle encompassing an ORC, liquified natural gas (LNG) power cycle, and a Rankine cycle. They also compared the role of the different working fluids in the ORC and found that the highest performance was accomplished using isopentane with optimum power production and cost rate of 179 kW and 19.3 $/h, respectively. Hoang [34] studied the economic, environmental, and thermodynamic aspects of recovering the heat wasted by a diesel engine using an ORC. He considered different configurations of the ORC and expressed that the energy efficiency using dual or multi-loop ORCs enhanced up to 60 %–90 %. Using the

response surface methodology (RSM), Boodaghi et al. [35] examined the feasibility of integrating an ORC with a heavy-duty diesel engine. They increased the net power output of the ORC by as much as 31 % of the power produced by the engine. Thus, the exergetic efficiency was found at 43 %. Choi et al. [36] worked on a diesel engine to improve its ability by means of a thermoelectric generator using a plate-type porous medium; its porosity was between 0.121 and 0.516. They stated that the porosity between 0.32 and 0.46 could maximize the net power output. Mohammad-khani et al. [37] investigated the potential of WHR in a diesel engine utilizing a Kalina cycle. They thermodynamically and economically examined the main parameters of the Kalina cycle on the performance whereby the exergetic efficiency and specific cost of power generated by the Kalina cycle were obtained at 55.5 % and 15.5 cent/kWh, respectively. Morawski et al. [38] comparatively studied the utilization of three WHR cycles, namely an ORC, a Rankine cycle, and a Kalina cycle, in integration with a Brazilian diesel engine power plant. Their study indicated good potential using the ORC, leading to generating 8.2 % (14.3 MW) further power. The heat wasted by a diesel engine was used to warm the water entering a solid oxide electrolyzer producing hydrogen by Wang wt al. [39]. The system was able to yield 22.4 kg/h hydrogen with an energy efficiency of 85.2 %; almost 12 % higher than the base system. Kolahi et al. [40] investigated the potential of WHR of a diesel engine employed in an offshore platform. They utilized two ORC-based configurations, i.e., simple ORC and ORC + internal heat exchanger, and evaluated the impact of different pure and zeotropic mixtures on the whole performance. They indicated that the best situation using the zeotropic mixture of R236ea/Cyclohexane led to the energetic and exergetic efficiencies of 16.8 % and 40.8 %, respectively. Also, its payback period was 13.45 years.

It is presented that the WHR is a crucial part of thermal engineering leading to increasing the potential of the applicability of

related prime movers [41]. Marine diesel engines (MDEs) are known as a group of widely used diesel engines. The WHR potential of them were analyzed in some studies. A trigeneration system encompassing a Kalina cycle, an ERC, and thermal processes-based desalination was joined to a MDE by Cao et al. [42] and analyzed thermodynamically. They studied the effect of some parameters on the performance of the system and indicated that the system was able to yield 1.3 kg/s desalinated water, 605 kW cooling, and 600 kW power. An experimental setup is designed by Yu et al. [43] to recover the waste heat of a MDE by a cascade ORC. They stated that the technique was able to improve the overall efficiency by 5.6 %. Bo et al. [44] thermodynamically and economically optimized a trigeneration system aimed to produce power, cooling, and desalinated by heat recovery for a MDE. The optimization of their work estimated the exergetic efficiency and cost rate of products were equal to 58 % and 66.7 $/GJ, respectively. Feili et al. [45] proposed a trigeneration system (hydrogen, power, and cooling) to establish in a ship working with the exhaust gas of its MDE. They also compared different zeotropic working fluids of the integrated cycle and stated that the use of Butene/Isopentane (0.35/0.65) made the highest exergy efficiency of 18.71 %. The integration of a regenerative ORC, an absorption chiller, and a desalination cycle was considered for multi heat recovery for a MDE. They analyzed and optimized the whole configuration and stated that the optimum exergetic efficiency was 43 % and optimum products' specific cost was 0.149 $/kWh. Shafeian and Khiadani [46] considered a framework for integrating a desalination cycle and an air-conditioning unit by waste heat recovery for a submarine design engine. They produced cooling up to 190 kW and stated that the production rate of the desalinated water is further sensitive to the temperature compared to the mass flow rate. In a study by Akman and Ergin [47], the thermodynamic and environmental aspects of using a transcritical ORC for WHR of a MDE were implemented. They showed that this technique improved the efficiency of the engine by around 2.5 %, and the system was able to reduce the carbon dioxide (CO_2) emission up to 678 tons/year. Cost and thermodynamic investigation and optimization of using a supercritical-CO_2 Brayton cycle for WHR of a marine diesel engine were accomplished by Pan et al. [48]. This study led to the optimum power output and energy and exergy efficiencies of 452 kW, 24.5 %, and 41.5 %, respectively. Gürgen and Altin [49] optimized the WHR process for a MDE using an ORC to identify the optimum operation using different organic working fluids. They stated that the best optimum power production capacity belonged to R600 with a value of 448.3 kW, and the best unit cost of electricity belonged to R245fa with a price of 0.057 $/kWh. Cao et al. [50] used an arrangement of an ORC, a chiller, and a desalination for waste heat recovery of a heavy MDE. They investigated the variability of the main performance metrics using a parametric study and obtained that the engine's efficiency was improved by 11.3 %. Also, the product's unit cost at the optimum state was reported to be 0.1494 $/kWh. Qu et al. [51] designed and thermodynamically investigated the potential of methane reforming integrated with a high-pressure exhaust gas recirculation system for a marine dual-fuel low-speed engine. The energy efficiency of 49.3 % and reduction of methane slip of 20 % were attained. In a study by Demir and Çıtakoğlu [52], a novel design of an onboard multigeneration process (hydrogen, electricity, water desalination, heating, and cooling) was proposed for a marine diesel engine. The system's overall exergy efficiency and the production capacity of freshwater and hydrogen were calculated at 13 %, 306.8 kg/day, and 0.536 kg/s, respectively. Wang et al. [53] utilized the waste heat of a marine diesel engine for a partial heating supercritical CO2 nested transcritical CO2 cascade power cycle. Thermodynamic, economic, and footprint analyses and optimization were conducted, and the optimal energy efficiency and unit cost of products were obtained at

29.3 % and 7.434 cent/kWh, respectively. In a study by Wang et al. [54], four different configurations of cooling and power cogeneration models were studied, optimized, and compared to each other. According to their results, the most suitable payback period was 5.8 years. Sun et al. [55] considered three different machine-learning algorithms to predict the operation of an absorption chiller driven by exhaust gas leaving a MDE. They want to keep the oration in a stable condition.

The literature review indicates that the use of WHR can increasingly affect the final performance of diesel engines. Thus, it is an appropriate opportunity to reuse the gas wasted during the operation of engines for higher performances based on producing further products. MDE is one of the most common diesel engines which operates during a variety of cruises with different purposes. It seems that its waste heat can be properly recovered to make different forms of energy and meet the energy needs of the ship and reduce the CO_2 emission. However, few models of WHR for MDEs have been proposed and examined previously, especially from the environmental perspective. In this regard, the current paper suggests a novel heat recovery process as an auxiliary cycle for a 1 MW MDE capable of producing further power and cooling simultaneously. This cycle comprises an absorption power cycle (APC) and an ERC combined with the exhaust gases leaving the MDE. This model is firstly introduced and examined in this paper. Thus, the exergetic, environmental, economic aspects of the system are examined and optimized accordingly. Toward this, an advanced evolutionary algorithm, i.e., a non-dominated sorting genetic algorithm, is considered to optimize the system concerning the exergetic efficiency and product's specific cost as objective functions. Also, the profitability of the system is analyzed by the net present value (NPV) method to find out its payback period.

2. Model description

The main configuration proposed in the current work is shown in Fig. 1 schematically. In addition to the MDE, there exsits an APC and ERC operating regularly.

The APC includes: a heat exchanger (HX), vapor generator 1 (VG1), a turbine, a solution heat exchanger (SHX), an absorber, pump 1 (pump I), and throttling valve 1 (T.V I).

The ERC includes: vapor generator 2 (VG 2), an ejector, a booster, an evaporator, a condenser, pump 2 (pump II), and throttling valve 2 (T.V II).

The MED regularly works with speed and torque of 1500 rpm and 6340 Nm with a power output of 1 MW, respectively. The stream wasted by the MDE is sent into the heat exchanger at point 25, where a part of its heat is transferred to stream 7. Afterward, the wasted stream goes into vapor generator 1 at point 26 and vapor generator 2 at point 27, respectively. Eventually, this stream is released into the atmosphere at point 28.

According to Fig. 1, the weak solution of the ammonia water (NH_3H_2O) conveys to vapor generator 1 and is separated into the water at point 7 and the strong solution at point 4. Accordingly, stream 7 is heated by the heat exchanger and flows into the turbine for power geneartion. Stream 9 at the turbine's outlet is sent into the absorber and dilutes the strong solution returned from to vapor generator 1. Consequently, stream 1 is formed and pumped into the solution heat exchanger (point 2), and gives the heat of stream 4 before entering vapor generator 1 at state 3.

In the ERC subsystem utilizing R410A working fluid, stream 13 is warmed by vapor generator 2 and is employed as the ejector's primary flow. Also, the booster provides its sucked stream at point 18, so stream 14 is sent into the condenser. Accordingly, the R410A is condensed at point 10 and is separated into streams 11 and 15. Stream 11 is pumped into vapor generator 2 and stream 15 by
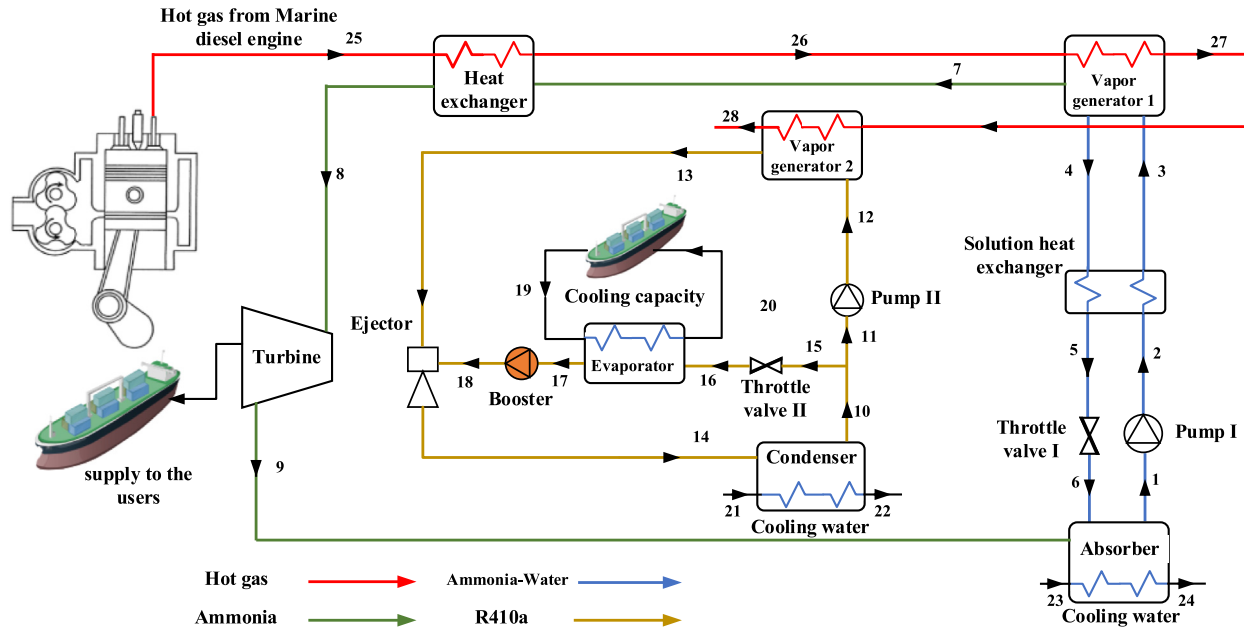
Fig. 1. The schematic layout of the cooling/power cogeneration system by the waste heat of MDE.

crossing throttling valve 2 enters the evaporator at point 16. Consequently, the required cooling is produced at point 20. Accordingly, stream 17 at the outlet of the evaporator flows into the booster and is delivered to the ejector at point 18.

3. Methodology

This study has been simulated and analyzed by the engineering equation solver (EES) and has been optimized by the NSGA-II method using MATLAB programming. The input data required to determine the outputs of the MDE have been calculated using the experimental results in Ref. [56]. The molar fraction of the compounds leaving the MED is written in Table 1.

Furthermore, Table 2 brings forward the input data of the study. The assumptions presented in the following assist the simulation of the arrangement planned in the current work.

- Considering a steady-state situation.
- Considering an isotropic efficiency for turbine, pumps, and booster.
- Considering a saturation state for the stream leaving the condenser and evaporator.
- Neglecting the change in the potential and kinetic energies and exergies.
- Neglecting the pressure loss and friction effect of the pipelines and heat exchangers on the analyses.
- Considering one-dimensional modeling for the ejector.
- Considering an adiabatic chamber of the ejector.
- Considering an isentropic efficiency for each part of the ejector.

- Neglecting the kinetic energy at the inlet and outlet terminals of the ejector.

As a whole, the steps of the simulation and analyses carried out during the study are shown in Fig. 2.

Table 1
Compounds of the exhaust gas leaving the engine [56].

Compound	Molecular weight (kg/kmol)	Molar fraction (%)
Steam (H_2O)	18.01	6.20
Carbon dioxide (CO_2)	44.00	4.36
Oxygen (O_2)	32.00	14.83
Nitrogen (N_2)	28.01	74.61

Table 2
Input data [45,57].

| Parameters	Value
Temperature of reference state, T_0 (K)	298.15
Pressure of reference state,P_0 (bar)	1.013
APC	
Temperature of vapor generator I,T_{VG1} (K)	413.15
Pressure of vapor generator I,P_{VGI} (bar)	22
Temperature of absorber,T_{ABS} (K)	303.15
Terminal temperature difference heat exchanger,ΔT_{HX} (K)	10
Ammonia concentration,$X_{ammonia}$ (%)	42
Isentropic efficiency of turbines,$\eta_{is,TUR}$ (%)	85
Isentropic efficiency of pump I, $\eta_{is,PUMI}$ (%)	85
Effectiveness of solution heat exchanger,ε_{SHE} (%)	82
ERC	
Terminal temperature difference Vapor generator II,ΔT_{VG2} (K)	10
Pressure of vapor generator II,P_{VG2} (bar)	25
Temperature of evaporator,T_{EVAP} (K)	278.15
Temperature of condenser,T_{COND} (K)	303. 15
Compression ratio of booster,CR_{boo}	1.8
Isentropic efficiency of pump II, $\eta_{is,PUMII}$ (%)	85
Isentropic efficiency of diffuser, $\eta_{is,dif}$ (%)	85
Isentropic efficiency of mixer, $\eta_{is,dif}$ (%)	85
Isentropic efficiency of nozzle,$\eta_{is,noz}$ (%)	90
Exergoeconomic parameters	
Annual operational in hours, N (h)	7000
Maintenance factor,φ_r	1.06
Yearly interest rate, i_r (%)	15
Lifetime,n_r(years)	20
Optimization	
Number of generations	100
Population size	500
Probability of crossover	0.8
Probability of mutation	0.01
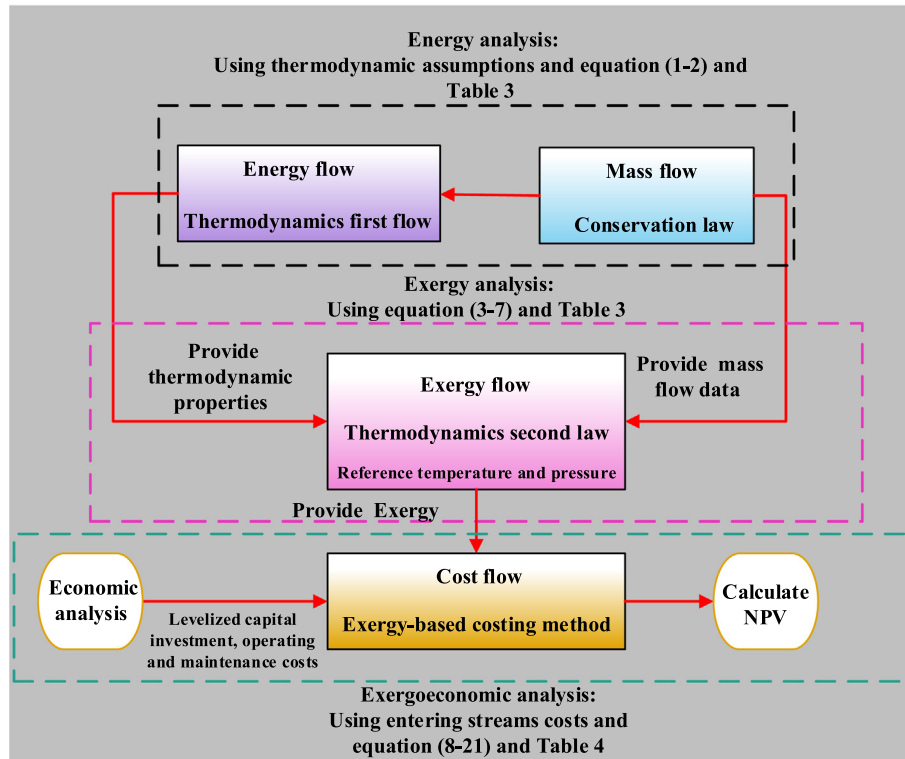
Fig. 2. Flowchart of the analyses implemented in this work.

3.1. Thermodynamic analysis

The first law of thermodynamics which exposes the energy rate balance is generally presented as equation (1) for the kth control volume [58,81]:

$$\dot{Q}_k - \dot{W}_k = \sum \dot{m}_{out,k} h_{out,k} - \sum \dot{m}_{in,k} h_{in,k} \tag{1}$$

where $\dot{Q}_k$ is the thermal energy rate, $\dot{W}_k$ is the work, $\sum \dot{m}_{out,k} h_{out,k}$ is the energy rate of the input streams, and

$\sum \dot{m}_{in,k} h_{in,k}$ is the energy rate of the output streams. Also, $\dot{m}$ and h stand for the mass rate and specific enthalpy, respectively.

The general mass balance rate of the kth control volume is written as [79,80]:

$$\sum \dot{m}_{in,k} = \sum \dot{m}_{out,k} \tag{2}$$

Table 3 exposes the equation of the first law of thermodynamic for each components of the scheme.

Accordingly, the second law of thermodynamic which determines the exergy concept is employed to evaluate the quality of the

Table 3
Energy and exergy relations for each components of the system [58,59].

Component	Energy balance relations	Exergy balance relations ($\dot{I}_{D,k}$)
Absorber	$\dot{Q}_{abs} = \dot{m}_6 h_6 + \dot{m}_9 h_9 - \dot{m}_1 h_1$, $\dot{Q}_{abs} = \dot{m}_{23}(h_{24} - h_{23})$	$(\psi_9 + \psi_6 - \psi_1) - (\psi_{24} - \psi_{23})$
Booster	$\dot{W}_{boo} = \dot{m}_{17}(h_{18} - h_{17})$, $\eta_{is,boo} = (h_{18s} - h_{17})/(h_{18} - h_{17})$	$\dot{W}_{boo} - (\psi_{18} - \psi_{17})$
Condenser	$\dot{Q}_{cond} = \dot{m}_{14}(h_{14} - h_{10})$, $\dot{Q}_{cond} = \dot{m}_{22}(h_{22} - h_{21})$	$(\psi_{14} - \psi_{10}) - (\psi_{22} - \psi_{21})$
TV I	$h_5 = h_6$	$\psi_5 - \psi_6$
TV II	$h_{15} = h_{16}$	$\psi_{15} - \psi_{16}$
Evaporator	$\dot{Q}_{eva} = \dot{m}_{17}(h_{17} - h_{16})$, $\dot{Q}_{eva} = \dot{m}_{19}(h_{19} - h_{20})$	$(\psi_{16} - \psi_{17}) - (\psi_{20} - \psi_{19})$
Nozzle section of ejector	$\mu = \frac{\dot{m}_{sf}}{\dot{m}_{pf}}$, $\eta_{noz} = \frac{h_{pf} - h_{noz}}{h_{pf} - h_{noz,is}}$, $h_{pf} - h_{noz} = \frac{1}{2}V_{noz}^2$	$(\psi_{13} + \psi_{18}) - \psi_{14}$
Mixing section of ejector	$V_{mf} = \frac{V_{noz}}{1+\mu}$, $\eta_{mix} = \frac{V_{mf,is}^2}{V_{mf}^2}$, $h_{out} - h_{mf} = \frac{1}{2}V_{mf,is}^2$	
Diffuser section of ejector	$h_{out} = \frac{h_{pf} + \mu h_{sf}}{1+\mu}$, $\eta_{dif} = \frac{h_{out,is} - h_{mf}}{h_{out} - h_{mf}}$	
HX	$\dot{Q}_{HX} = \dot{m}_7(h_8 - h_7)$, $\dot{Q}_{HX} = \dot{m}_{25}(h_{25} - h_{26})$ $\Delta T_{HE} = T_{25} - T_8$	$(\psi_{25} - \psi_{26}) - (\psi_8 - \psi_7)$
Pump I	$\dot{W}_{pu1} = \dot{m}_1(h_2 - h_1)$, $\eta_{is,pu1} = (h_{2s} - h_1)/(h_2 - h_1)$	$\dot{W}_{pu1} - (\psi_2 - \psi_1)$
Pump II	$\dot{W}_{pu2} = \dot{m}_{11}(h_{12} - h_{11})$, $\eta_{is,pu2} = (h_{12s} - h_{11})/(h_{12} - h_{11})$	$\dot{W}_{pu2} - (\psi_{12} - \psi_{11})$
SHE	$\dot{Q}_{SHX} = \dot{m}_4(h_4 - h_5)$, $\dot{Q}_{SHX} = \dot{m}_3(h_3 - h_2)$ $\varepsilon_{SHX} = (T_4 - T_5)/(T_4 - T_2)$	$(\psi_4 - \psi_5) - (\psi_3 - \psi_2)$
Turbine	$\dot{W}_{tur} = \dot{m}_8(h_8 - h_9)$, $\eta_{is,tur} = (h_8 - h_9)/(h_8 - h_{9s})$	$(\psi_8 - \psi_9) - \dot{W}_{tur}$
VG I	$\dot{m}_7 + \dot{m}_4 = \dot{m}_3$, $\dot{m}_3 X_3 = \dot{m}_4 X_4 + \dot{m}_7 X_7$, $\dot{Q}_{VGI} = \dot{m}_{26}(h_{26} - h_{27})$, $\dot{Q}_{VGI} = \dot{m}_4 h_4 + \dot{m}_7 h_7 - \dot{m}_3 h_3$,	$(\psi_{26} - \psi_{27}) - (\psi_7 + \psi_4 - \psi_3)$
VG II	$\dot{Q}_{VGII} = \dot{m}_{27}(h_{27} - h_{28})$, $\dot{Q}_{VGII} = \dot{m}_{13}(h_{13} - h_{12})$ $\Delta T_{VGII} = T_{27} - T_{13}$	$(\psi_{27} - \psi_{28}) - (\psi_{13} - \psi_{12})$

processes, components, and whole system. Generally, the exergy destruction rate of the kth control volume ($\dot{I}_{D,k}$) is written as [58,82]:

$$\dot{I}_{D,k} = \sum_j \left(1 - \frac{T_0}{T_j}\right)\dot{Q}_{j,k} - \dot{W}_k + \sum_i \psi_{in,k} - \sum_e \psi_{out,k} \tag{3}$$

or [30]

$$\dot{I}_{F,k} = \dot{I}_{D,k} + \dot{I}_{P,k} + \dot{I}_{L,k} \tag{4}$$

where $\dot{I}_{F,k}$, $\dot{I}_{P,k}$, and $\dot{I}_{L,k}$ refer to the exergy rate of the fuel and product of the kth control volume, and its exergy loss rate respectively.

The exergy rate of the ith stream (ψ_i) is divided into the physical (ph) and chemical (ch) forms as below [58]:

$$\psi_i = \psi_{ph,i} + \psi_{ch,i} \tag{5}$$

$$\psi_{ph,i} = \dot{m}_i\left((h_i - h_{0,i}) - T_0(s_i - s_{0,i})\right) \tag{6}$$

$$\psi_{ch,i} = \dot{n}_i\left(\sum y_j \bar{ex}_j^{ch,o} + \bar{R}T_0 \sum y_j ln(y_j)\right) \tag{7}$$

where s is the specific entropy, $\dot{n}$ is the molar rate, y_j is the molar fraction of jth compound within the ith stream, and $\bar{R}$ is the universal gas constant.

Table 3 entirely provides the related equation of exergy account of each component of the scheme.

3.2. Economic analysis

After the accounting the exergy, the exergoeconomic combines the exergy results with costs through the following cost balance equation [37,58]:

$$\dot{Z}_{k,PY} + \dot{C}_{\dot{Q}_k} - \dot{C}_{\dot{W}_k} = \sum \dot{C}_{out,k} - \sum \dot{C}_{in,k} \tag{8}$$

where $\dot{C}_{\dot{Q}_k}$ and $\dot{C}_{\dot{W}_k}$ display the cost rate of thermal loss and work of the kth control volume, respectively. Moreover, $\sum \dot{C}_{in,k}$ and $\sum \dot{C}_{out,k}$ refer to the cost rate of the input stream and output stream of the kth control volume, correspondingly.

Thus [37,58],

$$\dot{C}_{\dot{Q}_k} = c_{\dot{Q}_k}\left(1 - \frac{T_0}{T_j}\right)\dot{Q}_{j,k} \tag{9}$$

$$\dot{C}_{\dot{W}_k} = c_{\dot{W}_k}\dot{W}_k \tag{10}$$

$$\dot{C}_{in,k} = c_{in,k}\psi_{in,k} \tag{11}$$

$$\dot{C}_{out,k} = c_{out,k}\psi_{out,k} \tag{12}$$

Also, $\dot{Z}_{k,PY}$ is the kth control volume's updated investment cost rate [37,58].

$$\dot{Z}_{k,PY} = \dot{Z}_{k,RY}\frac{CI_{@PY}}{CI_{@RY}} \tag{13}$$

where $CI_{@PY}$ and $CI_{@RY}$ show the cost index of chemical plants at the present year and reference year, correspondingly. Also, $\dot{Z}_{k,RY}$ equals [37,58]:

$$\dot{Z}_{k,RY} = Z_k\frac{CRF\varphi}{N} \tag{14}$$

$$CRF = \frac{i_r(1+i_r)^n}{(1+i_r)^n - 1} \tag{15}$$

Here, Z_k, CRF, φ, and N are the purchase cost function, capital recovery factor, maintenance factor, and yearly operating time. Also, i_r and n denotes the annual interest rate and system's lifetime, respectively. Table 4 displays the related cost-based equation for each component.

The economic possibility, its profitability, and payback period are found by NPV method. On this path, the NPV equation depending on the fixed cost (FC) and annual saving money (AS) is [62]:

$$NPV = -FC + \sum_{m=1}^n (ASIF_m RDF_m) \tag{16}$$

Fixed cost is functioned by direct (DC) and indirect (IC) costs as below (see Ref. [41]).

$$FC = DC + IC \tag{17}$$

Also, annual saving money equals [62]:

$$AS = AI - OC \tag{18}$$

$$OC = 0.06FC \tag{19}$$

In the NPV equation, IF_m and RDF_m refer to the inflation factor and real discount factor. These factors are obtained by [62]:

$$IF_m = \left(1 + \frac{R}{100}\right)^{-m} \tag{20}$$

$$RDF_m = \left(1 + \frac{RIR}{100}\right)^{-m} \tag{21}$$

where R and RIR are the inflation rate and real interest rate, correspondingly.

3.3. Optimization procedure

Optimization can improve the quality of the process and reduce the cost of the designed configuration. Therefore, it is essential to add an optimization algorithm to the simulation of the system. On this account, the optimization procedure considered in this paper is NSGA-II coded by MATLAB programming. NSGA-II is a well-known, fast sorting, and elite multi objective genetic algorithm. Process parameters such as cutting speed, feed rate, rotational speed etc. are the considerable conditions in order to optimize the machining operations in minimizing or maximizing the machining performances. Unlike the single objective optimization technique, NSGA-II simultaneously optimizes each objective without being dominated by any other solution. NSGA-II is an advanced evolutionary algorithm depending on a smart search phenomenon with two principal features, namely crowding distance and non-dominated sorting [67]. Fig. 3 entirely shows the steps of the NSGA-II procedure.

This procedure has been utilized in several pertinent studies and its applicability has been proved significantly. Oyekale et al. [68] and Li et al. [69] utilized this method in solar thermal applications; in detail, a solar-based ORC and a solar-dish Brayton system, respectively. Cao et al. [70] employed a NSGA-II procedure for a direct-expansion solar-assisted heat pump. In a study by Rahdar et al. [71], energy storage air-conditioning systems using R717 and R134a were optimized through a NSGA-II. Jain et al. [72] proposed and optimized a vapor compression–absorption cascaded refrigeration system using a NSGA-II method. Yusuf et al. [73] evaluated its applicability for a system using photovoltaic cells and TEGs. Arora et al. [74] optimized a two-stage TEG via a NSGA-II method. Singh and Das [75,76], utilized this method in refrigeration applications.

Here, eight different decision variables are considered; their responsible variation range is reported in Table 5. These parame-

Table 4
Exergoeconomic relations for each components of the system [60–66].

| Component	Cost balance relation	Auxiliary relation	Purchase cost function
Absorber	$\dot{C}_9 + \dot{C}_{23} + \dot{C}_6 + \dot{Z}_{abs} = \dot{C}_{24} + \dot{C}_1$	$(\dot{C}_9 + \dot{C}_6)/(\psi_9 + \psi_6) = c_1$ $c_{23} = 0$	$Z_{abs} = 130(\frac{A_{abs}}{0.093})^{0.78}$
Booster	$\dot{C}_{13} = \dot{C}_{W,boo} + \dot{C}_{12} + \dot{Z}_b$	$c_{W,b} = c_{w,pu2}$	$Z_{boo} = 9624.2\dot{W}_{boo}^{0.46}$
Condenser	$\dot{C}_{10} + \dot{C}_{22} = \dot{C}_{14} + \dot{C}_{21} + \dot{Z}_{cond}$	$c_{10} = c_{14}, c_{21} = 0$	$Z_{cond} = 130(\frac{A_{cond}}{0.093})^{0.78}$
TV I	$\dot{C}_6 = \dot{C}_5 + \dot{Z}_{TVI}$	–	$Z_{TVI} = 114.5 \times \dot{m}_5$
TV II	$\dot{C}_{12} = \dot{C}_{11} + \dot{Z}_{TVI}$	–	$Z_{TVII} = 114.5 \times \dot{m}_{15}$
Evaporator	$\dot{C}_{20} + \dot{C}_{17} = \dot{C}_{19} + \dot{C}_{16} + \dot{Z}_{eva}$	$c_{16} = c_{17}, c_{19} = 0$	$Z_{eva} = 130(\frac{A_{eva}}{0.093})^{0.78}$
Ejector	$\dot{C}_{14} = \dot{C}_{13} + \dot{C}_{18} + \dot{Z}_{eje}$	–	$\dot{Z}_{eje} = 0$
HX	$\dot{C}_7 + \dot{C}_{25} + \dot{Z}_{HX} = \dot{C}_{26} + \dot{C}_8$	$c_{25} = c_{26}$ $c_{25} = 23.59$[44]	$Z_{HE} = 130(\frac{A_{HE}}{0.093})^{0.78}$
Pump I	$\dot{C}_2 = \dot{C}_{w,pu1} + \dot{C}_1 + \dot{Z}_{pu1}$	$c_{w,pu1} = c_{w,tur}$	$Z_{pu1} = 2100(\frac{\dot{W}_{pu1}}{10})^{0.26}(\frac{1-\eta_{is,pu}}{\eta_{is,pu}})^{0.5}$
Pump II	$\dot{C}_{12} = \dot{C}_{w,pu2} + \dot{C}_{11} + \dot{Z}_{pu2}$	$c_{w,pu2} = c_{w,tur}$	$Z_{pu2} = 2100(\frac{\dot{W}_{pu2}}{10})^{0.26}(\frac{1-\eta_{is,pu}}{\eta_{is,pu}})^{0.5}$
SHE	$\dot{C}_4 + \dot{C}_2 + \dot{Z}_{SHE} = \dot{C}_5 + \dot{C}_3$	$c_4 = c_5$	$Z_{SHE} = 130(\frac{A_{SHEhx}}{0.093})^{0.78}$
Turbine	$\dot{C}_9 + \dot{C}_{w,tur} = \dot{C}_8 + \dot{Z}_{tur}$	$c_1 = c_2$	$Z_{tur} = 4405\dot{W}_{tur}^{0.7}$
VG I	$\dot{C}_{26} + \dot{C}_3 + \dot{Z}_{VGI} = \dot{C}_4 + \dot{C}_7 + \dot{C}_{27}$	$c_{26} = c_{27}$ $a = \frac{\dot{C}_4}{(\psi_4 - \psi_3)} b = \frac{\dot{C}_3(\psi_7 - \psi_4)}{(\psi_4 - \psi_3)(\psi_7 - \psi_3)} c = \frac{\dot{C}_7}{(\psi_7 - \psi_3)} a - b - c = 0$	$Z_{VGI} = 130(\frac{A_{VGI}}{0.093})^{0.78}$
VG II	$\dot{C}_{12} + \dot{C}_{27} + \dot{Z}_{VGII} = \dot{C}_{13} + \dot{C}_{28}$	$c_{27} = c_{28}$	$Z_{VGII} = 130(\frac{A_{VGII}}{0.093})^{0.78}$
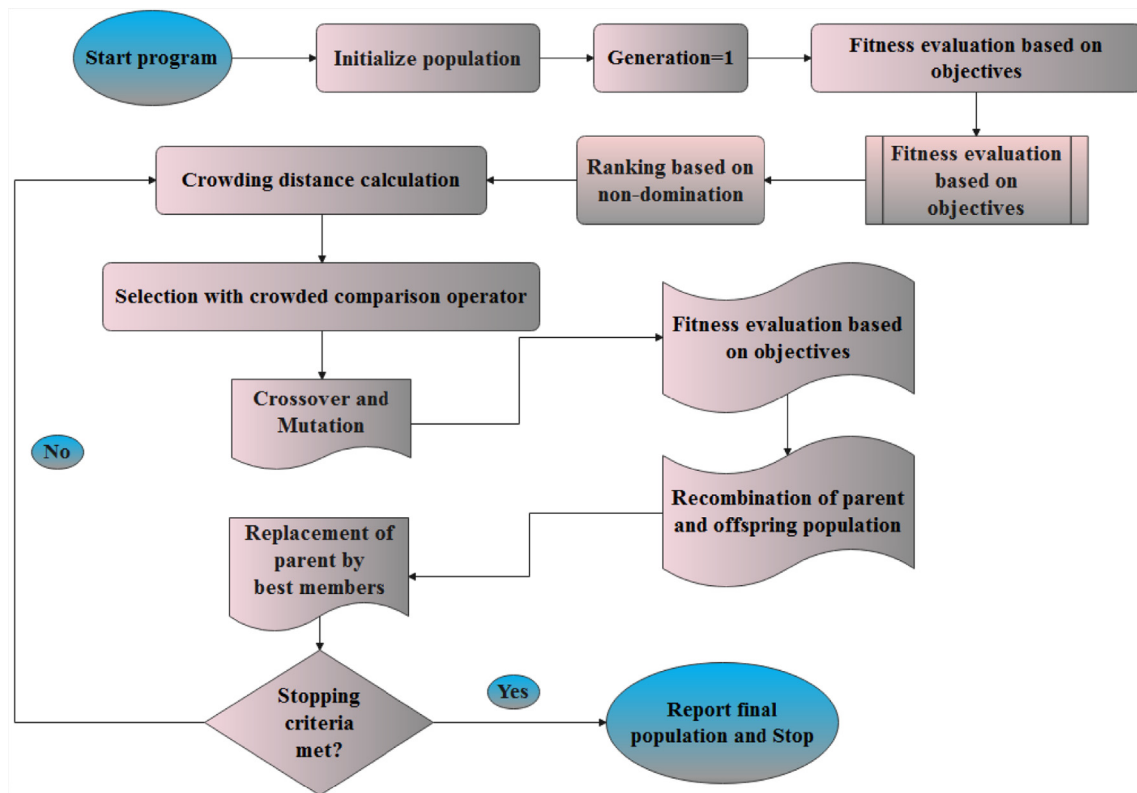
Fig. 3. Flowchart of the NSGA-II optimization procedure.

Table 5
Decision variables and their reasonable ranges.

Pressure of VG I	$15 \leq P_{VGI}$ (bar) ≤ 25
Pressure of VG II	$20 \leq P_{VGII}$ (bar) ≤ 30
Ammonia concentration	$0.35 \leq X_{ammonia} \leq 0.55$
Compression ratio of booster	$1.5 \leq CR_{boo} (-) \leq 2.5$
Terminal temperature difference of HX	$5 \leq \Delta T_{HX}(K) \leq 30$
Terminal temperature difference VG I	$5 \leq \Delta T_{VGI}(K) \leq 30$
Temperature of VG I	$393.15 \leq T_{VGI}(K) \leq 423.15$
Temperature of evaporator	$276.15 \leq T_{eva}(K) \leq 280.15$

ters and their limitation range are considred according to two main points: similar studies and limitations of the simulation governing our newly designed process. With regard to the proposed system in this paper, the principal parameters affecting the capacity of products and thermo-economic facets are regarded. However, the logic of thermal simulation in the present study and the convergence conditions of the equations lead to the settings presented in Table 5. The objective functions of the current research are the exergetic efficiency of the system (η_{ex}) and total unit cost of products (TUCP).

The Pareto frontier generated by the NSGA-II is evaluated by the TOPSIS decision making to find out the best solution. This decision making is a technique with respect to the normalized and weighted matrixes of responses to the objective functions, which depend on the best and worst distances formulated by:

$$S_i^+ = \sqrt{\sum_{j=1}^{n}(v_{ij} - v_j^+)^2} \qquad (22)$$

$$S_i^- = \sqrt{\sum_{j=1}^{n}(v_{ij} - v_j^-)^2} \qquad (23)$$

Here, S_i^+ refers to the distance of each state from the ideal solution, S_i^- is the distance of each state from the non-ideal solution, and v_j^+ and v_j^- are the best and the worst responses to the jth objective, respectively. According to the TOPSIS, the best point is found at:

$$i_{final} = i \in max(Y_i) \qquad (25)$$

where

$$Y_i = \frac{S_i^-}{S_i^- + S_i^+} \qquad (26)$$

4. Results and discussion

This chapter has been provided in three subchapters containing, model verification, sensitivity analysis results, and the results of the NSGA-II optimization. The performance variables studied in this study are introduced and formulated in Table 6.

4.1. Model verification

There are two main subsystems, namely APC and ERC that need to be validated. Thus, the verification of their model has been conducted in comparison with the literature and has been provided in Tables 7 and 8. According to Table 7, the performance variables of the APC involving energetic and exergetic efficiencies, mass flow rate of the stream entering the turbine, duty of vapor generator, turbine output power, and power consumption of the pump are obtained and compared with the study by Shokati et al. [77]. This comparison is considered for a net power of 1 MW. The mean relative error measured is below 1.5 %. Moreover, the performance variables of the ERC based on the heat duty of the vapor generator and evaporator, mass entrainment ratio, and COP are computed and compared by the Śmierciew et al. [78] study in Table 8. Here, the maximum relative error is below 3.5 %. Thus, it is inferred the model developed is verified by high accuracy.

Table 6
Formulation of the performance variables [37,58].

Performance variable	Formula
Net power output	$\dot{W}_{net} = \dot{W}_{tur} - \dot{W}_{PUMI} - \dot{W}_{PUMII} - \dot{W}_{boo}$
Cooling output	$\dot{Q}_{cooling} = \dot{m}_{19}(h_{19} - h_{20})$
Energetic efficiency	$\eta_{en} = \frac{\dot{W}_{net} + \dot{Q}_{cooling}}{\dot{m}_{25}(h_{25} - h_{28})}$
Exergetic efficiency	$\eta_{ex} = \frac{\dot{W}_{net} + (\psi_{19} - \psi_{20})}{\psi_{25}}$
Total unit cost of products	$TUCP = \frac{\dot{C}_{\dot{W}_{net}} + \dot{C}_{20}}{\dot{W}_{net} + \dot{\psi}_{20}}$
CO2 emission reduction	$CER = \frac{\dot{m}_{gas}y_{CO2}}{\dot{W}_{MDE}} - \frac{\dot{m}_{gas}y_{CO2}}{\dot{W}_{MDE} + \dot{W}_{net} + \dot{Q}_{cooling}}$
Cost rate of exergy loss	$\dot{C}_L = \dot{C}_{22} + \dot{C}_{24} + \dot{C}_{28}$
Cost rate of exergy destruction	$\dot{C}_D = c_{25}\dot{I}_{D,total}$
Total investment cost rate	$\dot{Z}_{total} = \sum_{k=1}^{n}\dot{Z}_{K,PY}$
Exergoeconomic factor	$f = \frac{\dot{Z}_{total}}{\dot{Z}_{total} + \dot{C}_L + \dot{C}_D}$

Table 7
Validation of the APC with Ref. [77].

Variable	Ref. [77]	This study	Relative error (%)
Energetic efficiency (%)	10.71	10.49	2.1 %
Exergetic efficiency (%)	36.12	36.26	0.4
Turbine's inlet flow rate (kg/s)	4.36	4.23	1.5
Duty of vapor generator (MW)	9.36	9.35	0.1
Turbine output power (kW)	1048	1046	0.2
Consumption of pump (kW)	48	46	4.2

$P_{VG} = 20\,(bar),\ T_{in,VG} = 150\,(°C),\ X_{ammonia} = 0.4, T_{abs} = 50\,(°C)$

Table 8
Validation of the ERC with Ref. [78].

Variable	Ref. [78]	This study	Relative error (%)
Vapor generator duty (kW)	9	8.713	3.18
Cooling output (kW)	1.75	1.706	2.51
Coefficient of performance (-)	0.19	0.1954	2.84
Entrainment ratio (-)	0.24	0.2422	0.91

4.2. Results of sensitivity analysis

The exergetic, environmental, and economic performance variables are studied by varying the working pressure of VG I (P_{VGI}) and VG II (P_{VGII}), ammonia mass fraction ($X_{ammonia}$), and booster's compression ratio (CR_{boo}). These variables include η_{ex}, $TUCP$, $\dot{Z}_{total}$, $\dot{C}_D + \dot{C}_L$, f, and CER where Figs. 4-7 indicate the change in the performance variables mentioned with regard to the parameters used.

In Fig. 4, the effect of the P_{VGI} (from 20 to 25 bar) is studied on the performance variables, and attained curves are plotted accordingly. As can be evident from Fig. 4, the η_{ex} goes down, while other variables experience an increase continuously. From the perspective of the change in the production rate of products, the upsurge in the P_{VGI} declines the net power output and augments the cooling output inversely. This is because of the negative effect of this variation on the mass flow rate of water at point 7. Therefore, the input mas flow rate of the turbine goes down and reduces its production capacity. Also, the heat input to the ERC augments, leading to generating further cooling. Since η_{ex} is more influenced by the net power output, it has a reducing trend from 31.8 % to 30.0 %. Also, the $TUCP$ experiences an increase from 58.3 $/GJ to 60.3 $/GJ. This behavior owes to the reduction in the products' lower exergy rates at higher pressures. The increase in the heat input of the ERC increases the size and capacity of its components; this behavior affects the $\dot{Z}_{total}$ and rises this variable from 3.02 $/h to 3.15 $/h. Subsequently, the $\dot{C}_D + \dot{C}_L$ also enhances from 14.44 $/h to 14.49 $/h; this is because of the enhancement of the system's irreversibility by decreasing the η_{ex}. Since the $\dot{Z}_{total}$ is further varied by P_{VGI} compared to the $\dot{C}_D + \dot{C}_L$, the variable f faces an increment from 27.29 % to 27.57 %. Eventually, CER increases from 21.2 kg/MWh to 22.2 kg/MWh due to decreasing the energy level of products.

The performance variables are assessed with P_{VGII} (from 25 to 30 bar) in Fig. 5. It is indicated that the η_{ex} witnesses a decrement from 31.45 % to 31.05 %. This variation increases the power consumed by pump II, so the power consumption capacity of the system goes up. Therefore, the net output power undergoes a decrement imposing a similar trend for the η_{ex}. Here, the $TUCP$ rises from 58.8 $/GJ to 59.8 $/GJ owing to the decrease in the exergy level of outputs. Similar to increasing P_{VGI}; here, the size and capacity of the ERC's components increase with P_{VGII} resulting in higher $\dot{Z}_{total}$ at higher pressures. So, this variable rises from 3.07 $/h to 3.15 $/h. Accordingly, the $\dot{C}_D + \dot{C}_L$ witnesses an increment from 14.44 $/h to 14.49 $/h due to the reason stated in the previous paragraph. Consequently, variable f augments from 27.4 % to 27.8 %, as well.
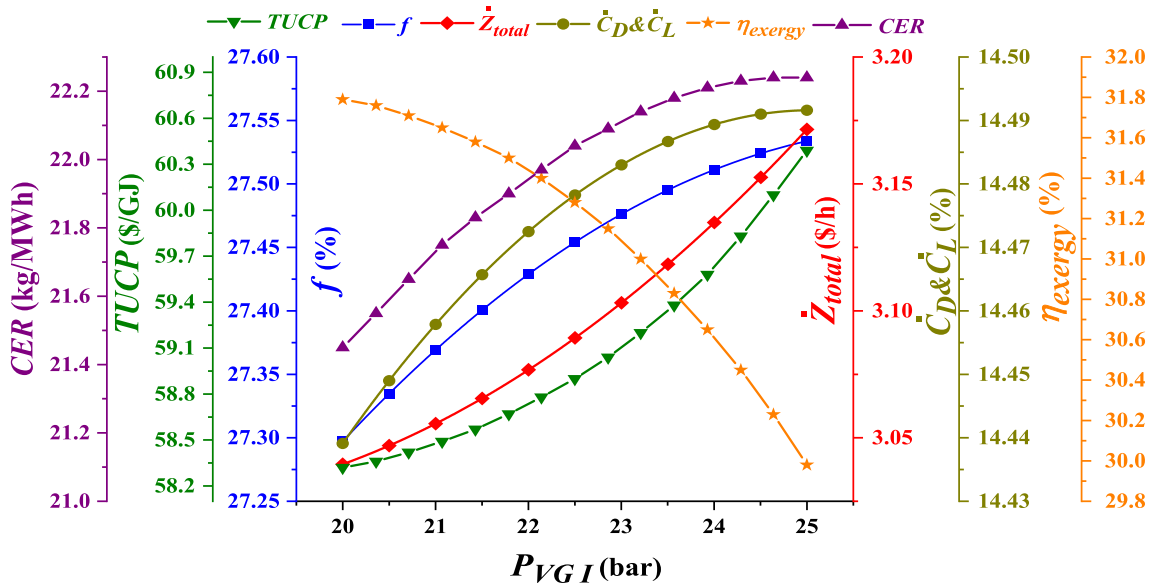
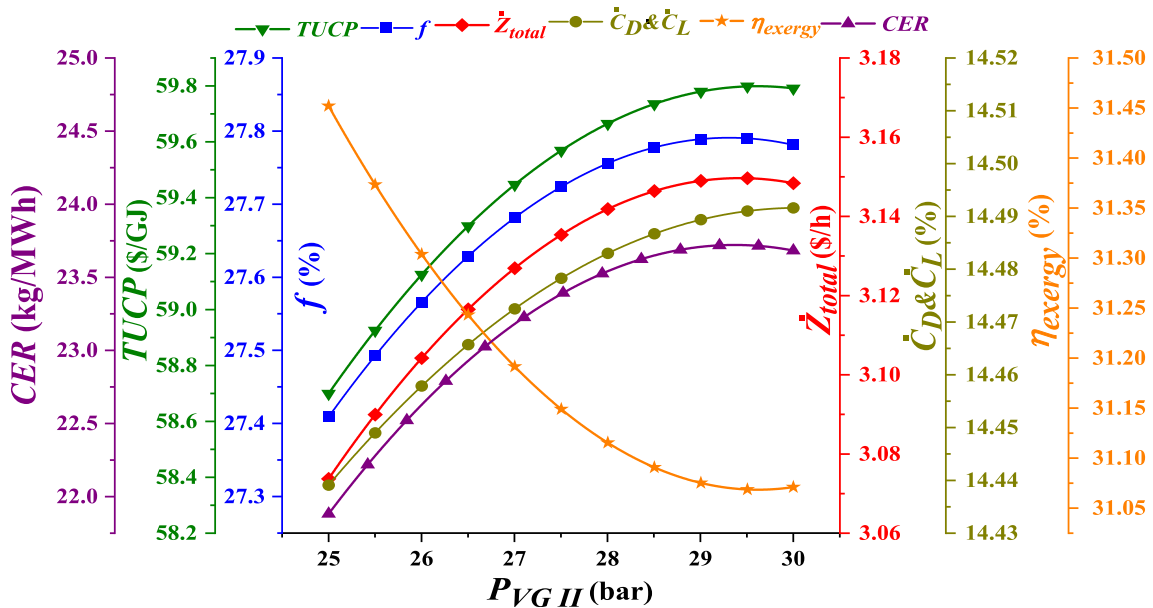**Fig. 4.** Variation in performance variables with P_{VGI}.

Fig. 5. Variation in performance variables with P_{VGII}.

From the environmental perspective, the variation in this pressure increases the CER from 21.8 kg/MWh to 23.7 kg/MWh. Because the output rate of products declines.

The $X_{ammonia}$ (from 0.35 to 0.55) at the outlet of the absorber is another parameter used for evaluating the performance variables (see Fig. 6). Generally speaking, this parameter affects the operation of the APC through which other cycles are affected as well. It variation strongly affects the output power of the turbine by which this variable faces an increasing–decreasing trend. Since trend of the η_{ex} strongly depends on the behavior of the output power of the turbine, η_{ex} behaves similarly. Here, the highest $\eta_{ex} = 32.0\%$ occurs at $X_{ammonia} = 0.46$. Afterward, the heat duty of VG I augments; in contrast, the enthalpy rate of the hot stream

entering VG II declines. So, the decline in the cooling output is justifiable. According to the logical contradiction between the exergy rate of products and their cost rate, the $TUCP$ faces a reduction from 64.2 \$/GJ to 54.6 \$/GJ. In addition, the ERC's components size and capacity reduce, diminishing the $\dot{Z}_{total}$ from 3.25 \$/h to 2.70 \$/h. Also, the $\dot{C}_D + \dot{C}_L$ declines at first, then increases slightly. This trend strongly depends on the trend of the η_{ex} showing the circumstance of the irreversibility of the system. Here, the least $\dot{C}_D + \dot{C}_L$ equals 14.25 \$/h at $X_{ammonia} = 0.45$. Due to the sharp variation in the $\dot{C}_D + \dot{C}_L$ compared to the $\dot{Z}_{total}$, the variable f augments up to 65.0 % at $X_{ammonia} = 0.43$, then declines up to 55.2 % at $X_{ammonia} = 0.45$. From the environmental perspective, the highest $CER = 22.2$ kg/MWh.
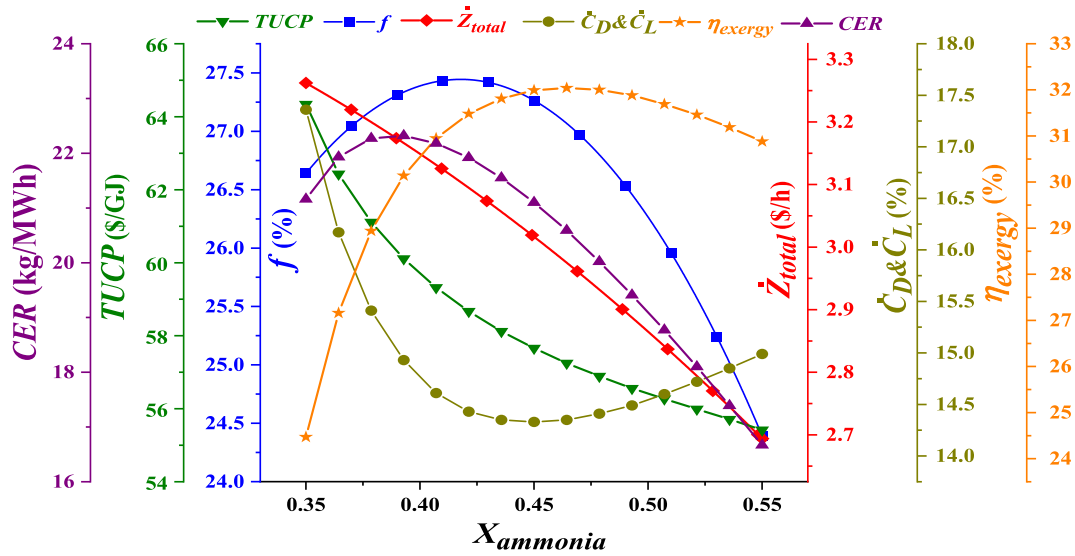
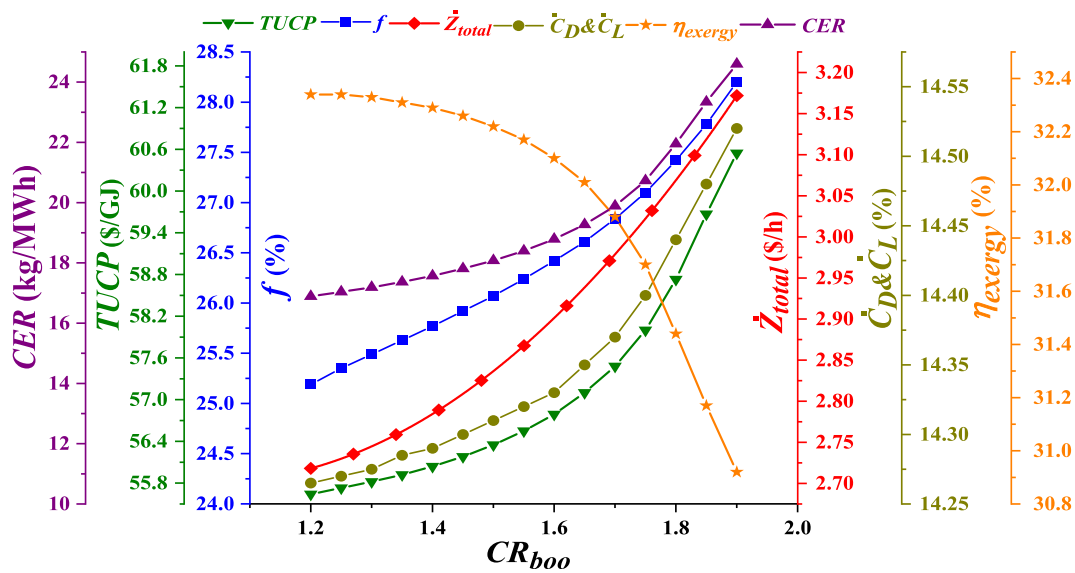**Fig. 6.** Variation in performance variables with $X_{ammonia}$.

Fig. 7. Variation in performance variables with CR_{boo}.

The last parameter introduced in the current study is CR_{boo} (from 1.2 to 1.9) which evaluates the performance parameters in Fig. 7. Referring to Fig. 7, the η_{ex} witnesses a decline and other variables experience an increase. In principle, the increase in this parameter enhances the ejector's mass entrainment ratio, so the cooling output augments. Despite this, the power consumed by the booster increases; thus, the net power output of the system undergoes a reduction. Affected by the reduction in net power output of the system, η_{ex} declines from 32.4 % to 30.9 %. Besides, the exergy level of the outputs diminishes augmenting the $TUCP$ from 55.8 $/GJ to 60.6 $/GJ. Accordingly, the $\dot{Z}_{total}$ escalates from 2.72 $/h to 3.17 $/h which owes to the enhancement of the size and capacity of the components utilized in the ERC section. The $\dot{C}_D + \dot{C}_L$ also faces an increase in contrast with the η_{ex} from 14.26 $/h to 14.57 $/h. Consequently, the sharp increase in the $\dot{Z}_{total}$ enhances the vari-

able f from 25.2 % to 28.3 %. Moreover, the CER increase from 16.8 kg/MWh to 24.5 kg/MWh.

4.3. Results of the NSGA-II optimization

The procedure of the NSGA-II has been coded by MATLAB programming and has been used to optimize the operation of the system using eight decision variables and two objective functions. On this path, the objectives selected include η_{ex} and $TUCP$ whereby the Pareto frontier achieved by the NSGA-II is plotted in Fig. 8. On this plot, points A and B are corresponding to the lowest $TUCP$ and the highest η_{ex} of 50.1 $/GJ and 38.19 %, respectively. Despite this, the best solution is designated by the TOPSIS decision making, where the optimum $\eta_{ex} = 35.2\%$ and the optimum $TUCP = 53.01/GJ$.
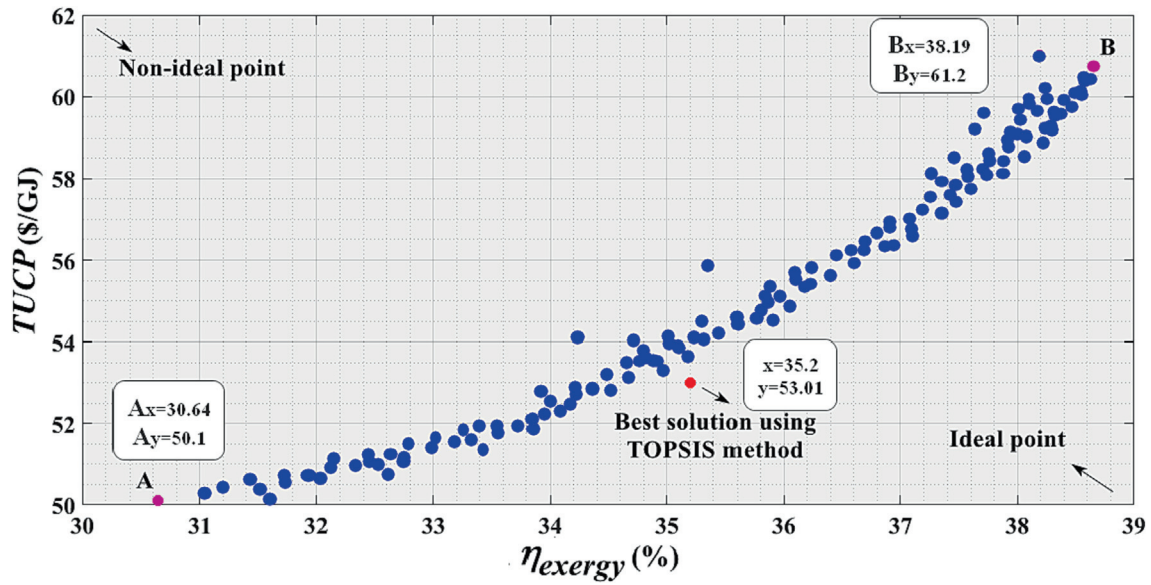
Fig. 8. Pareto frontier obtained by NSGA-II.

Table 9
Comparing the results between the base case and optimum state.

Decision variables	Base case	Best solution	Performance variables	Base case	Best solution
P_{VGI} (bar)	22	24.6	$\dot{W}_{net}$ (kW)	54.3	61.5
P_{VGII} (bar)	25	20.1	$\dot{Q}_{eva}$ (kW)	20.9	12.1
$X_{ammonia}(\%)$	0.42	0.45	$\eta_{en}(\%)$	17.70	17.29
$CR_{boo}(-)$	1.8	1.69	$\eta_{ex}(\%)$	31.44	35.19
ΔT_{HX} (K)	10	5.4	$\dot{I}_L$ (kW)	23.99	23.52
ΔT_{VGI} (K)	10	12.7	$\dot{I}_D$ (kW)	95.87	89.75
T_{VGI} (K)	413.15	422.9	$CER(kg/MWh)$	21.95	21.5
T_{eva} (K)	278.15	278.8	$TUCP(/GJ)$	58.73	53.01
			$\dot{C}_D$ (/h)	8.14	7.62
			$\dot{C}_L$ (/h)	6.30	5.90
			$\dot{Z}_{total}$ (/h)	3.08	2.80
			$f(\%)$	27.42	26.85

Table 10
Optimum thermodynamic properties of each state.

State	T(K)	P(kPa)	h(kg/kJ)	s(kg/kJ K)	$\dot{m}$(kg/s)	ψ(kW)	c(/kWh)	$\dot{C}$(/h)
1	303.2	2.816	0.3007	−103.4	0.6464	7.332	0.1703	1.249
2	303.4	24.62	0.3022	−100.3	0.6464	9.014	0.1818	1.639
3	378.4	24.62	1.309	241.9	0.6464	36.27	0.3931	14.26
4	422.9	24.62	1.861	483.2	0.4988	48.05	0.2827	13.58
5	324.9	24.62	0.6709	39.69	0.4988	3.738	0.2827	1.057
6	325.3	2.816	0.6785	39.69	0.4988	2.605	0.4061	1.058
7	422.9	24.62	5.731	1772	0.1476	71.68	0.1592	11.41
8	567.8	24.62	6.516	2159	0.1476	94.17	0.1457	13.72
9	383.2	2.816	6.645	1729	0.1476	24.99	0.1457	3.642
10	303.2	18.89	1.164	248.3	0.08515	7.503	0.4906	3.68
11	303.2	18.89	1.164	248.3	0.08331	7.341	0.4906	3.601
12	303.2	20.1	1.164	248.4	0.08331	7.351	0.4907	3.607
13	370.7	20.1	1.979	504.4	0.08331	8.433	0.4766	4.019
14	368.1	18.89	1.982	503	0.08515	8.437	0.4906	4.139
15	303.2	18.89	1.164	248.3	0.001833	0.1615	0.4906	0.07923
16	278.7	9.519	1.173	248.3	0.001833	0.1566	0.5059	0.07923
17	278.8	9.519	1.8	423	0.001833	0.1344	0.5059	0.06797
18	306.9	16.05	1.808	439.3	0.001833	0.1599	0.7505	0.12
19	298.2	1.013	0.3669	104.8	0.004656	0	0	0
20	281.7	1.013	0.1297	36.07	0.004656	0.009167	1.409	0.01292
21	298.2	1.013	0.3669	104.8	0.5264	0	0	0
22	308	1.013	0.5029	146	0.5264	0.3505	1.36	0.4767
23	298.2	1.013	0.3669	104.8	8.296	0	0	0
24	308	1.013	0.5029	146	8.296	5.525	0.7102	3.924
25	573.2	1.013	7.702	−828.5	1.983	174.8	0.08492	14.85
26	546.8	1.013	7.65	−857.3	1.983	147.9	0.08492	12.56
27	383.4	1.013	7.271	−1032	1.983	22.4	0.08492	1.902
28	373.2	1.013	7.243	−1043	1.983	17.67	0.08492	1.5

Table 9 reports the set of decision variables by which the optimum circumstance is found. Furthermore, the optimum values of performance variables are calculated and presented, and are compared with those of the base case (the information of the base case is reported in Table 2). According to this table, the optimum set of decision variables is defined at $P_{VGI} = 24.6$ bar, $P_{VGII} = 20.1$ bar, $X_{ammonia} = 0.45$, $CR_{boo} = 1.69$, $\Delta T_{HX} = 5.4$K, $\Delta T_{VGI} = 12.7$K, $T_{VGI} = 422.9$K, and $T_{eva} = 278.8$K. Besides, the optimum capacity of net power and cooling are 61.5 kW and 12.1 kW, correspondingly. Besides, the optimum state provides the $= 21.5$ kg/MWh, $\dot{Z}_{total} = 2.80$/h, $\dot{C}_D + \dot{C}_L = 13.52$/h, and $f = 26.85\%$.

Eventually, the thermodynamic properties including temperature, pressure, specific enthalpy, specific entropy, mass flow rate, and exergy rate of each point of the system with respect to the optimum point selected by TOPSIS are regularly presented in Table 10.

Fig. 9 reveals the exergy flow diagram through a Sankey illustration. Through this figure, the variation in exergetic performance of components against the input exergy rate of the system is shown. As can be evident, the total input exergy rate equals 174.8 kW where 61.53 kW is recovered by the system. Here, VG I has the maximum exergy destruction rate of 42.08 kW. Also, the exergy loss rate of the system is computed at 23.54 %.

Accordingly, Fig. 10 proves the cost balance of the system at the optimum state. Here, the total cost rate of the input fuel is 14.85 $/h, and the total investment cost rate is 2.8 $/h, where the products' cost rate and exergy loss cost rate are obtained at 11.74 $ and 5.9 $/h, respectively.

The results of the NPV examination are revealed in Fig. 11. This figure is plotted for selling prices of the power and cooling outputs in the optimum state and base case. According to Fig. 11, it can be seen that the optimum circumstance diminishes the payback period up to 6.79 years. The payback period takes place in a year where the NPV = 0. This duration is 14.2 % lower compared to the base case with a payback period of 7.91 years, as well.
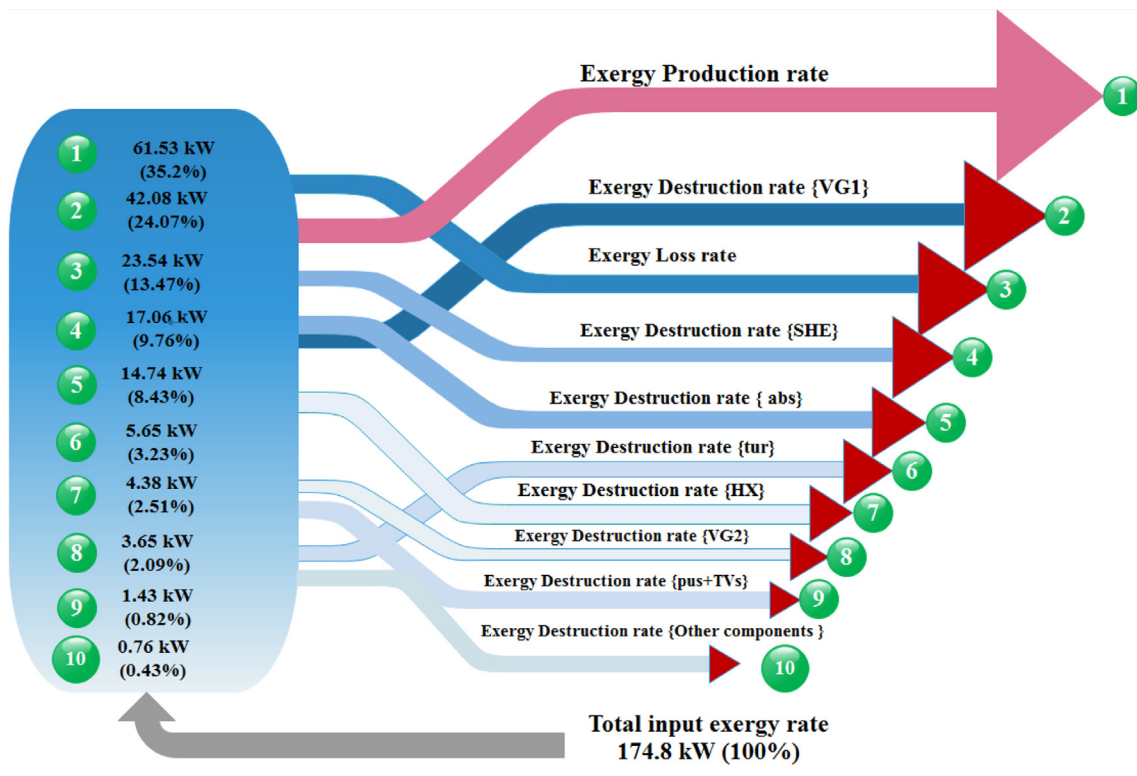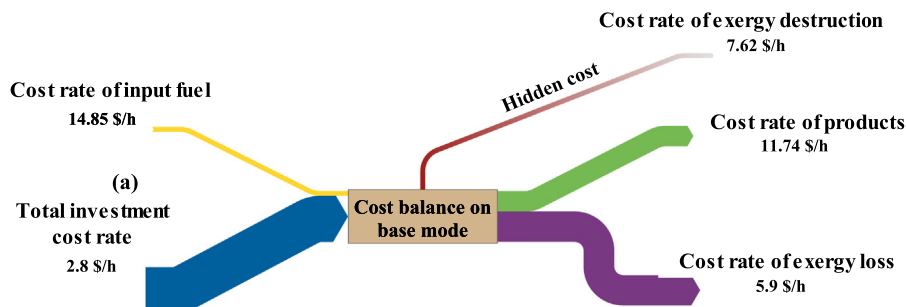

Fig. 9. Exergy flow diagram at the optimum state.

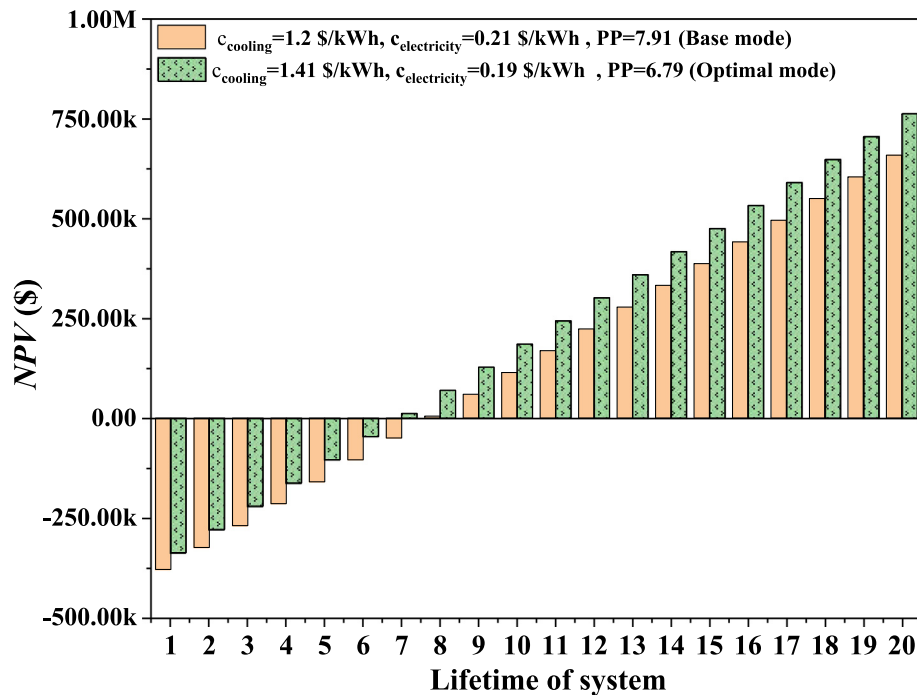

Fig. 10. Cost flow diagram at the optimum state.

Fig. 11. NPV results of the system at the optimum state.

Table 11
Compsring the outcomes of this study with the literature review.

Refernce	Engine type	Subsystems	Analysis type	Optimization type	Main outcomes
Xia et al. [31]	Diesel engine	CO_2 Brayton cycle ORC ERC	Thermodynamic Exergoeconomic	Genetic algorithm	η_{ex} = 27.6 % $TUCP$ = 63.5 \$/MWh
Mohammadkhani et al. [37]	Diesel engine	Kalina cycle	Thermodynamic Exergoeconomic	Without optimization	η_{en} = 25.5 %, η_{ex} = 55.5 % PUC = 15.52 cent/kWh
Kolahi et al. [40]	Diesel engine	ORC	Thermodynamic Exergoeconomic NPV	Without optimization	η_{en} = 16.8 % η_{ex} = 40.8 % $TUCP$ = 10.48 k\$/kW PP = 13.3 years
Bo et al. [44]	MDE	Kalina cycle ERC Desalination	Thermodynamic Exergoeconomic .	Genetic algorithm	η_{en} = 81 %, η_{ex} = 49 % $TUCP$ = 78.6 \$/GJ
Feili et al. [45]	MDE	ORC Bi-evaporator cycle Water electolysis unit	Thermodynamic	Without optimization	η_{en} = 22.1 %, η_{ex} = 18.7 %
Pan et al. [48]	MDE	S-CO_2 Brayton cycle	Thermodynamic Exergoeconomic Environmental	Imperialist Competitive Algorithm	η_{en} = 24.5 % η_{ex} = 41.5 % EUC = 0.005 \$/kWh
Cao et al. [50]	MDE	ORC Chiller Desalination	Thermodynamic Exergoeconomic	Genetic algorithm	η_{en} = 58.4 % η_{ex} = 43.0 % $TUCP$ = 0.1494 \$/kWh.
This study	MDE	APC ERC	Thermodynamic Environmental Exergoeconomic NPV	NGGA-II	η_{en} = 17.29 % η_{ex} = 35.19 % CER = 21.5kg/MWh $TUCP$ = 53.01 \$/GJ PP = 6.79 years

4.4. Comparing the results

The outcomes of the current study are compared with the literature in this subsection. In this regard, Table 11 is provided. Detailed information can be found referring to this table.

5. Conclusions

This work was motivated to design a small-scale power/cooling cogeneration arrangement regarding a carbon dioxide emission reduction (*CER*) scheme based on a waste-to-energy process for its diesel engine. Hence, a combined framework of an absorption power cycle/ejector refrigeration cycle (APC/ERC) was designed and joined to the engine. The exergetic, environmental, and economic evaluations along with a multi-criteria optimization were done. Here, a non-dominated sorting genetic algorithm (NSGA-II) was applied; the objective functions included exegetic efficiency (η_{ex}) and total unit cost of products (*TUCP*). Also, the net present value (NPV) was forecasted to realize the profitability and payback period of the configuration. The main findings of this work are presented next. environmental.

- The sensitivity analysis showed that the exergetic and economic performance metrics were more impacted by the variation in $X_{ammonia}$ and CER by CR_{boo}. There was an extremum point for the η_{ex} (the maximum point), f (the maximum point), $\dot{C}_D + \dot{C}_L$ (the minimum point), and CER (the maximum point) regarding the variation range of the $X_{ammonia}$. Also, $TUCP$ and $\dot{Z}_{total}$ faced a reduction with $X_{ammonia}$.
- The increase in P_{VGI} and P_{VGII} slightly varied the performance variables. The exergy efficiency is declined and other variables increased by P_{VGI} and P_{VGII}. Similar behaviors were also seen with changing CR_{boo} but were meaningful.
- The optimum state deduced by the TOPSIS deduced making demonstrated optimum $\eta_{ex} = 35.19\%$ and $TUCP = 53.01/GJ$. These objectives were respectively 3.75 percent-point and 9.7 % higher compared to the base case. In addition, the optimum CER was equal to 29.5 kg/MWh.
- The $\dot{Z}_{total}$ and $\dot{C}_D + \dot{C}_L$ reduced up to 2.8 \$/h and 13.52 \$/h through the NSGA-II optimization. These values were 9.1 % and 6.4 % lower than the base case.
- The payback period of the optimum state was 6.79 year; 14.2 % lower than the base case.

Declaration of Competing Interest

The authors declare that they have no known competing financial interests or personal relationships that could have appeared to influence the work reported in this paper.

Acknowledgments

References

[1] Varshil P, Deshmukh D. A comprehensive review of waste heat recovery from a diesel engine using organic rankine cycle. Energy Rep 2021;7:3951–70.

[2] Liu W, Liu L, Wu H, Chen Y, Zheng X, Li N, et al. Performance analysis and offshore applications of the diffuser augmented tidal turbines. Ships and Offshore Struct 2022:1–10.

[3] Xia C, Zhu Y, Zhou S, Peng H, Feng Y, Zhou W, et al. Simulation study on transient performance of a marine engine matched with high-pressure SCR system. Int J Engine Res 2022. 14680874221084052.

[4] Wang Y, Wang H, Zhou B, Fu H. Multi-dimensional prediction method based on Bi-LSTMC for ship roll. Ocean Eng 2021;242:110106.

[5] Lü C, Sun Q, Zhang W, Geng J, Qi Y, Lu L. The effect of high temperature on tensile strength of sandstone. Appl Therm Eng 2017;111:573–9.

[6] Chang H, Han Z, Li X, Ma T, Wang Q. Experimental study on heat transfer performance of sCO2 near pseudo-critical point in airfoil-fin PCHE from viewpoint of average thermal-resistance ratio. Int J Heat Mass Transf 2022;196:123257.

[7] Cui W, Si T, Li X, Li X, Lu L, Ma T, et al. Heat transfer analysis of phase change material composited with metal foam-fin hybrid structure in inclination container by numerical simulation and artificial neural network. Energy Rep 2022;8:10203–18.

[8] (a) Yang, M., Li, C., Luo, L., Li, R., & Long, Y. (2021). Predictive model of convective heat transfer coefficient in bone micro-grinding using nanofluid aerosol cooling. International Communications in Heat and Mass Transfer, 125, 105317. (b) Gao, T., Li, C., Yang, M., Zhang, Y., Jia, D., Ding, W., ... & Wang, J. (2021).

[9] Mahmoudi A, Fazli M, Morad MR. A recent review of waste heat recovery by Organic Rankine Cycle. Appl Therm Eng 2018;143:660–75.

[10] Haghghi MA, Holagh SG, Pesteei SM, Chitsaz A, Talati F. On the performance, economic, and environmental assessment of integrating a solar-based heating system with conventional heating equipment; a case study. Therm Sci Eng Prog 2019;13:100392.

[11] Gao T, Li C, Yang M, Zhang Y, Jia D, Ding W, et al. Mechanics analysis and predictive force models for the single-diamond grain grinding of carbon fiber reinforced polymers using CNT nano-lubricant. J Mater Process Technol 2021;290:116976.

[12] Zhang J, Li C, Zhang Y, Yang M, Jia D, Liu G, et al. Experimental assessment of an environmentally friendly grinding process using nanofluid minimum quantity lubrication with cryogenic air. J Clean Prod 2018;193:236–48.

[13] Tang L, Zhang Y, Li C, Zhou Z, Nie X, Chen Y, et al. Biological stability of water-based cutting fluids: Progress and application. Chinese J Mech Eng 2022;35 (1):1–24.

[14] Li B, Li C, Zhang Y, Wang Y, Jia D, Yang M. Grinding temperature and energy ratio coefficient in MQL grinding of high-temperature nickel-base alloy by using different vegetable oils as base oil. Chin J Aeronaut 2016;29(4):1084–95.

[15] Said Z, Arora S, Farooq S, Sundar LS, Li C, Allouhi A. Recent advances on improved optical, thermal, and radiative characteristics of plasmonic nanofluids: Academic insights and perspectives. Sol Energy Mater Sol Cells 2022;236:111504.

[16] Jouhara H, Khordehgah N, Almahmoud S, Delpech B, Chauhan A, Tassou SA. Waste heat recovery technologies and applications. Therm Sci Eng Prog 2018;6:268–89.

[17] Ejaz A, Babar H, Ali HM, Jamil F, Janjua MM, Fattah IR, et al. Concentrated photovoltaics as light harvesters: Outlook, recent progress, and challenges. Sustain Energy Technol Assess 2021;46:101199.

[18] Zhang D, Li C, Zhang Y, Jia D, Zhang X. Experimental research on the energy ratio coefficient and specific grinding energy in nanoparticle jet MQL grinding. Int J Adv Manuf Technol 2015;78(5):1275–88.

[19] Jia D, Li C, Zhang Y, Yang M, Zhang X, Li R, et al. Experimental evaluation of surface topographies of NMQL grinding ZrO2 ceramics combining multiangle ultrasonic vibration. Int J Adv Manuf Technol 2019;100(1):457–73.

[20] Holagh SG, Haghghi MA, Chitsaz A. Which methane-fueled fuel cell is of superior performance in CCHP applications; solid oxide or molten carbonate? Fuel 2022;312:122936.

[21] Haghghi MA, Holagh SG, Chitsaz A, Parham K. Thermodynamic assessment of a novel multi-generation solid oxide fuel cell-based system for production of electrical power, cooling, fresh water, and hydrogen. Energ Conver Manage 2019;197:111895.

[22] Forman C, Muritala IK, Pardemann R, Meyer B. Estimating the global waste heat potential. Renew Sustain Energy Rev 2016;57:1568–79.

[23] Zhou J, Hai T, Ali MA, Shamseldin MA. Sattam Fahad Almojil, Abdulaziz Ibrahim Almohana, Abdulrhman Fahmi Alali, Waste heat recovery of a wind turbine for poly-generation purpose: Feasibility analysis, environmental impact assessment, and parametric optimization. Energy Part D 2023;263:125891. doi: https://doi.org/10.1016/j.energy.2022.125891.

[24] Li CH, Li JY, Wang S, Zhang Q. Modeling and numerical simulation of the grinding temperature field with nanoparticle jet of MQL. Adv Mech Eng 2013;5:986984.

[25] Said Z, Ghodbane M, Boumeddane B, Tiwari AK, Sundar LS, Li C, et al. Energy, exergy, economic and environmental (4E) analysis of a parabolic trough solar collector using MXene based silicone oil nanofluids. Sol Energy Mater Sol Cells 2022;239:111633.

[26] Said Z, Jamei M, Sundar LS, Pandey AK, Allouhi A, Li C. Thermophysical properties of water, water and ethylene glycol mixture-based nanodiamond+ Fe3O4 hybrid nanofluids: An experimental assessment and application of data-driven approaches. J Mol Liq 2022;347:117944.

[27] Said Z, Sundar LS, Rezk H, Nassef AM, Chakraborty S, Li C. Thermophysical properties using ND/water nanofluids: An experimental study, ANFIS-based model and optimization. J Mol Liq 2021;330:115659.

[28] Anqi AE, Li C, Dhahad HA, Sharma K, Attia EA, Abdelrahman A, Rajhi AA. Effect of combined air cooling and nano enhanced phase change materials on thermal management of lithium-ion batteries. J Storage Mater 2022;52:104906.

[29] Zhu S, Zhang K, Deng K. A review of waste heat recovery from the marine engine with highly efficient bottoming power cycles. Renew Sustain Energy Rev 2020;120:109611.

[30] Sadeghi M, Mahmoudi SMS, Saray RK. Exergoeconomic analysis and multi-objective optimization of an ejector refrigeration cycle powered by an internal combustion (HCCI) engine. Energ Conver Manage 2015;96:403–17.

[31] Xia J, Wang J, Lou J, Zhao P, Dai Y. Thermo-economic analysis and optimization of a combined cooling and power (CCP) system for engine waste heat recovery. Energ Conver Manage 2016;128:303–16.

[32] Yang F, Cho H, Zhang H, Zhang J, Wu Y. Artificial neural network (ANN) based prediction and optimization of an organic Rankine cycle (ORC) for diesel engine waste heat recovery. Energ Conver Manage 2018;164:15–26.

[33] Habibi H, Zoghi M, Chitsaz A, Javaherdeh K, Ayazpour M. Thermo-economic analysis and optimization of combined PERC-ORC-LNG power system for diesel engine waste heat recovery. Energy Convers Canagem 2018;173:613–25.

[34] Hoang AT. Waste heat recovery from diesel engines based on Organic Rankine Cycle. Appl Energy 2018;231:138–66.

[35] Boodaghi H, Etghani MM, Sedighi K. Performance analysis of a dual-loop bottoming organic Rankine cycle (ORC) for waste heat recovery of a heavy-duty diesel engine, Part I: Thermodynamic analysis. Energ Conver Manage 2021;241:113830.

[36] Choi Y, Negash A, Kim TY. Waste heat recovery of diesel engine using porous medium-assisted thermoelectric generator equipped with customized thermoelectric modules. Energ Conver Manage 2019;197:111902.

[37] Mohammadkhani F, Yari M, Ranjbar F. A zero-dimensional model for simulation of a Diesel engine and exergoeconomic analysis of waste heat recovery from its exhaust and coolant employing a high-temperature Kalina cycle. Energ Conver Manage 2019;198:111782.

[38] Morawski AP, de Araújo LR, Schiaffino MS, de Oliveira RC, Chun A, Ribeiro LC, et al. On the suitable superstructure thermoeconomic optimization of a waste heat recovery system for a Brazilian diesel engine power plant. Energ Conver Manage 2021;234:113947.

[39] Wang F, Wang L, Ou Y, Lei X, Yuan J, Liu X, et al. Thermodynamic analysis of solid oxide electrolyzer integration with engine waste heat recovery for hydrogen production. Case Stud Therm Eng 2021;27:101240.

[40] Kolahi M, Yari M, Mahmoudi SMS, Mohammadkhani F. Thermodynamic and economic performance improvement of ORCs through using zeotropic mixtures: case of waste heat recovery in an offshore platform. Case Stud Therm Eng 2016;8:51–70.

[41] Feili M, Hasanzadeh M, Ghaebi H, Abdi Aghdam E. Comprehensive analysis of a novel cooling/electricity cogeneration system driven by waste heat of a marine diesel engine. Energy Sources Part A 2022;44(3):7331–46.

[42] Cao Y, Mihardjo LW, Dahari M, Mohamed AM, Ghaebi H, Parikhani T. Assessment of a novel system utilizing gases exhausted from a ship's engine for power, cooling, and desalinated water generation. Appl Therm Eng 2021;184:116177.

[43] Yu G, Shu G, Tian H, Huo Y, Zhu W. Experimental investigations on a cascaded steam-/organic-Rankine-cycle (RC/ORC) system for waste heat recovery (WHR) from diesel engine. Energ Conver Manage 2016;129:43–51.

[44] Bo Z, Mihardjo LW, Dahari M, Abo-Khalil AG, Al-Qawasmi AR, Mohamed AM, et al. Thermodynamic and exergoeconomic analyses and optimization of an auxiliary tri-generation system for a ship utilizing exhaust gases from its engine. J Clean Prod 2021;287:125012.

[45] Feili M, Rostamzadeh H, Parikhani T, Ghaebi H. Hydrogen extraction from a new integrated trigeneration system working with zeotropic mixture, using waste heat of a marine diesel engine. Int J Hydrogen Energy 2020;45(41):21969–94.

[46] Shafieian A, Khiadani M. A multipurpose desalination, cooling, and air-conditioning system powered by waste heat recovery from diesel exhaust fumes and cooling water. Case Stud Therm Eng 2020;21:100702.

[47] Akman M, Ergin S. Thermo-environmental analysis and performance optimisation of transcritical organic Rankine cycle system for waste heat recovery of a marine diesel engine. Ships Offshore Struct 2021;16(10):1104–13.

[48] Pan P, Yuan C, Sun Y, Yan X, Lu M, Bucknall R. Thermo-economic analysis and multi-objective optimization of S-CO2 Brayton cycle waste heat recovery system for an ocean-going 9000 TEU container ship. Energ Conver Manage 2020;221:113077.

[49] Gürgen S, Altin İ. Novel decision-making strategy for working fluid selection in Organic Rankine Cycle: A case study for waste heat recovery of a marine diesel engine. Energy 2022;124023.

[50] Cao Y, Delpisheh M, Yousefiasl S, Athari H, El-Shorbagy MA, Jarad F, et al. Examination and optimization of a novel auxiliary trigeneration system for a ship through waste-to-energy from its engine. Case Stud Therm Eng 2022;31:101860.

[51] Qu J, Feng Y, Xu G, Zhang M, Zhu Y, Zhou S. Design and thermodynamics analysis of marine dual fuel low speed engine with methane reforming integrated high pressure exhaust gas recirculation system. Fuel 2022;319:123747.

[52] Demir ME, Çıtakoğlu F. Design and modeling of a multigeneration system driven by waste heat of a marine diesel engine. Int J Hydrogen Energy 2022.

[53] Wang Z, Jiang Y, Ma Y, Han F, Ji Y, Cai W. A partial heating supercritical CO2 nested transcritical CO2 cascade power cycle for marine engine waste heat recovery: Thermodynamic, economic, and footprint analysis. Energy 2022;261:125269.

[54] Wang Z, Mo X, Qin P, Zhao Z, Ouyang T. Multi-dimensional assessment and multi-objective optimization of electricity-cooling cogeneration system driven by marine diesel engine waste heat. J Clean Prod 2022;334:130187.

[55] Sun Y, Sun P, Zhang Z, Zhang S, Zhao J, Mei N. Performance Prediction for a Marine Diesel Engine Waste Heat Absorption Refrigeration System. Energies 2022;15(19):7070.

[56] Song J, Song Y, Gu CW. Thermodynamic analysis and performance optimization of an Organic Rankine Cycle (ORC) waste heat recovery system for marine diesel engines. Energy 2015;82:976–85.

[57] Hasanzadeh A, Chitsaz A, Mojaver P, Ghasemi A. Stand-alone gas turbine and hybrid MCFC and SOFC-gas turbine systems: Comparative life cycle cost, environmental, and energy assessments. Energy Rep 2021;7:4659–80.

[58] Moran MJ, Shapiro HN, Boettner DD, Bailey MB. Fundamentals of engineering thermodynamics. John Wiley & Sons; 2010.

[59] Parikhani T, Delpisheh M, Haghghi MA, Holagh SG, Athari H. Performance enhancement and multi-objective optimization of a double-flash binary geothermal power plant. Energy Nexus 2021;2:100012.

[60] Delpisheh M, Haghghi MA, Mehrpooya M, Chitsaz A, Athari H. Design and financial parametric assessment and optimization of a novel solar-driven freshwater and hydrogen cogeneration system with thermal energy storage. Sustain Energy Technol Assess 2021;45:101096.

[61] Cao Y, Dhahad HA, Togun H, Haghghi MA, Athari H, Mohamed AM. Exergetic and economic assessments and multi-objective optimization of a modified solar-powered CCHP system with thermal energy storage. J Build Eng 2021;43:102702.

[62] Athari H, Kiasatmanesh F, Haghghi MA, Teymourzadeh F, Yagoublou H, Delpisheh M. Investigation of an auxiliary option to meet local energy demand via an innovative small-scale geothermal-driven system; a seasonal analysis. J Build Eng 2022;50:103902.

[63] Cao Y, Dhahad HA, Togun H, Haghghi MA, Anqi AE, Farouk N, et al. Seasonal design and multi-objective optimization of a novel biogas-fueled cogeneration application. Int J Hydrogen Energy 2021;46(42):21822–43.

[64] Holagh SG, Haghghi MA, Mohammadi Z, Chitsaz A. Exergoeconomic and environmental investigation of an innovative poly-generation plant driven by a solid oxide fuel cell for production of electricity, cooling, desalinated water, and hydrogen. Int J Energy Res 2020;44(13):10126–54.

[65] Farajollahi A, Rostami M, Feili M, Ghaebi H, Salimi MR. Modified cost analysis integrated with dual parametric sensitivity study for realistic cost assessment of a novel modified geothermal-based multi-generation energy system. Energy Rep 2022;8:13463–83.

[66] Haghghi MA, Mohammadi Z, Pesteei SM, Chitsaz A, Parham K. Exergoeconomic evaluation of a system driven by parabolic trough solar collectors for combined cooling, heating, and power generation; a case study. Energy 2020;192:116594.

[67] Yusoff Y, Ngadiman MS, Zain AM. Overview of NSGA-II for optimizing machining process parameters. Procedia Eng 2011;15:3978–83.

[68] Oyekale J, Petrollese M, Cau G. Multi-objective thermo-economic optimization of biomass retrofit for an existing solar organic Rankine cycle power plant based on NSGA-II. Energy Rep 2020;6:136–45.

[69] Li Y, Liao S, Liu G. Thermo-economic multi-objective optimization for a solar-dish Brayton system using NSGA-II and decision making. Int J Electr Power Energy Syst 2015;64:167–75.

[70] Cao Y, Mihardjo LW, Parikhani T. Thermal performance, parametric analysis, and multi-objective optimization of a direct-expansion solar-assisted heat pump water heater using NSGA-II and decision makings. Appl Therm Eng 2020;181:115892.

[71] Rahdar MH, Heidari M, Ataei A, Choi JK. Modeling and optimization of R-717 and R-134a ice thermal energy storage air conditioning systems using NSGA-II and MOPSO algorithms. Appl Therm Eng 2016;96:217–27.

[72] Jain V, Sachdeva G, Kachhwaha SS, Patel B. Thermo-economic and environmental analyses based multi-objective optimization of vapor compression–absorption cascaded refrigeration system using NSGA-II technique. Energ Conver Manage 2016;113:230–42.

[73] Yusuf A, Bayhan N, Tiryaki H, Hamawandi B, Toprak MS, Ballikaya S. Multi-objective optimization of concentrated Photovoltaic-Thermoelectric hybrid system via non-dominated sorting genetic algorithm (NSGA II). Energ Conver Manage 2021;236:114065.

[74] Arora R, Kaushik SC, Arora R. Multi-objective and multi-parameter optimization of two-stage thermoelectric generator in electrically series and parallel configurations through NSGA-II. Energy 2015;91:242–54.

[75] Singh K, Das R. Improved quantification of exergy destruction in mechanical cooling tower considering all tower inlet parameters. J Heat Transfer 2018;140(5).

[76] Singh K, Das R. Simultaneous optimization of performance parameters and energy consumption in induced draft cooling towers. Chem Eng Res Des 2017;123:1–13.

[77] Shokati N, Ranjbar F, Yari M. A comparative analysis of rankine and absorption power cycles from exergoeconomic viewpoint. Energ Conver Manage 2014;88:657–68.

[78] Śmierciew K, Gagan J, Butrymowicz D, Karwacki J. Experimental investigations of solar driven ejector air-conditioning system. Energ Build 2014;80:260–7.

[79] Jafary S, Shawabkeh SKA. MakatarWae-hayee, Mehran Hashemian, A complete energetic and exergetic analysis of a solar powered trigeneration system with two novel organic Rankine cycle (ORC) configurations. J Clean Prod 2021;281:. doi: https://doi.org/10.1016/j.jclepro.2020.124552124552.

[80] Mohammad Jalili, Ata Chitsaz, Mehran Hashemian, Marc A. Rosen, Economic and environmental assessment using emergy of a geothermal power plant, Energy Convers Manage, 228, 152021, 113666. https://doi.org/10.1016/j.enconman.2020.113666.

[81] Mehran Hashemian, Samad Jafarmadar, El-Shorbagy M.A. Anas A.Rahman, Mahidzal Dahari, Makatar Wae-hayee, Efficient heat extraction from the storage zone of solar pond by structurally improved spiral pipes; numerical simulation/experimental validation. Energy Rep 8(2022):7386–7400. https://doi.org/10.1016/j.egyr.2022.05.247.

[82] Mehran Hashemian, Samad Jafarmadar, HamdiAyed, Makatar Wae-hayee Thermal-hydrodynamic and exergetic study of two-phase flow in helically coiled pipe with helical wire insert. Case Stud Therm Eng 30(2022):101718. https://doi.org/10.1016/j.csite.2021.101718.

Makatar Wae-hayee received the Bachelor of Industrial Technology in Mechanical Technology from Rajamangala University of Technology Srivijaya (rmutsv), Thailand (2005). He also received Master of Engineering in Mechanical Engineering from Prince of Songkhla University (PSU), Thailand (2007). Then, he started his Doctor of Philosophy in Mechanical Engineering in Prince of Songkhla University (PSU), Thailand and received his Ph.D. in 2014. Currently, he is Assistant Professor in Department of Mechanical and Mechatronics Engineering, Faculty of Engineering, Prince of Songkla University, Thailand. His fields of interest are Combustion, Gasification, Biomass conversion, Thermal-Fluid Engineering, Heat and Mass Transfer, Computational Fluid Dynamic (CFD), Food drying